THE JOURNAL OF PHYSICAL CHEMISTRY LETTERS
A JOURNAL OF THE AMERICAN CHEMICAL SOCIETY

pubs.acs.org/JPCL

Letter

Ultrafast Excited-State Dynamics of Photoluminescent Pt(II) Dimers Probed by a Coherent Vibrational Wavepacket

Pyosang Kim, Andrew J. S. Valentine, Subhangi Roy, Alexis W. Mills, Arnab Chakraborty, Felix N. Castellano,* Xiaosong Li,* and Lin X. Chen*

Cite This: https://doi.org/10.1021/acs.jpclett.1c01289

Read Online

ACCESS | Metrics & More | Article Recommendations | Supporting Information

ABSTRACT: Intricate potential energy surfaces (PESs) of some transition metal complexes (TMCs) pose challenges in mapping out initial excited-state pathways that could influence photochemical outcomes. Ultrafast intersystem crossing (ISC) dynamics of four structurally related platinum(II) dimer complexes were examined by detecting their coherent vibrational wavepacket (CVWP) motions of Pt−Pt stretching mode in the metal-metal-to-ligand-charge-transfer excited states. Structurally dependent CVWP behaviors (frequency, dephasing time, and oscillation amplitudes) were captured by femtosecond transient absorption spectroscopy, analyzed by short-time Fourier transformation, and rationalized by quantum mechanical calculations, revealing dual ISC pathways. The results suggest that the ligands could fine-tune the PESs to influence the proximity of the conical intersections of the excited states with the Franck−Condon state and thus to control the branching ratio of the dual ISC pathways. This comparative study presents future opportunities in control excited-state trajectories of TMCs via ligand structures.

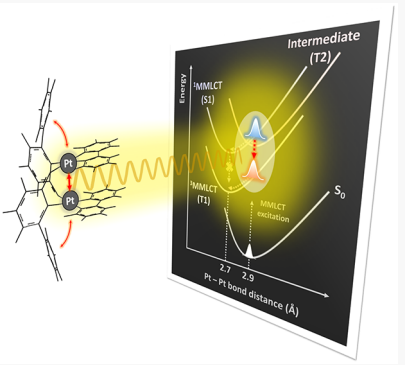

Transition metal complexes (TMCs) have played important roles in solar energy conversion, photocatalysis, and optoelectronics because of their versatile excited-state properties.[1−8] Although extensive studies have been carried out to tune TMC excited states by chemical synthesis for desirable photochemical reactions, how these excited states evolve on the intricate potential energy surfaces (PESs) in real time to influence the reaction outcome has not been fully explored until recently.[9−16] It has been well recognized that excited-state trajectories on the femtosecond time scale are defined by dynamic interplays between electronic and nuclear structures well before thermalization or vibrational relaxation. Hence, the vibronic coupling should be included in mechanistic descriptions related to the ultrafast excited-state dynamics of TMCs.

Excited-state vibrational quantum coherence comes from an impulsive excitation into multiple vibrational levels, generating coherent vibrational wavepacket (CVWP) motions whose time evolution behaviors, such as oscillation frequency and amplitude, could be used to map out excited-state trajectories. Ultrafast studies of photoactive TMCs have reported CVWP dynamics associated with structural rearrangements in excited-state processes, such as intersystem crossing (ISC).[9−16] These studies demonstrated that excited states of TMCs travel intricate pathways due to the interplay between vibrational and electronic degrees of freedom on the ultrafast time scale.[11,15,17−19] Hence, capturing vibrational quantum coherence in the excited-state TMCs can open up possibilities to reveal and optimize the excited-state trajectories leading to optimal reaction outcomes.[1,20,21]

Pt(II) complexes have shown promise in applications of organic light-emitting diodes and photocatalysts.[22−24] Previous studies of cyclometalated Pt(II) dimer complexes with a pseudo-2-fold symmetry demonstrated structurally tunable photophysical properties.[25] As the Pt−Pt distance decreases in the ground state due to stereohindrance exerted by the bridging ligand, the lowest-energy electronic transition transforms from a ligand-centered (LC) and/or metal-to-ligand-charge-transfer (MLCT) transition localized on one-half of the molecule to a metal-metal-to-ligand-charge-transfer (MMLCT) transition delocalized over the entire molecule.[25−30] As the Pt(II)−Pt(II) distance decreases, the interactions of the $5d_{z^2}$ molecular orbitals (MOs) between the two Pt(II) atoms become stronger, causing a larger energy splitting between the dσ bonding MO and dσ* antibonding MO (HOMO) and thus increasing the HOMO energy. Consequently, the lowest-energy electronic transition is transformed to the MMLCT in nature, dominated by the HOMO(dσ*)−LUMO(π*) transitions and red-shifted in the ground-state absorption spectra.[25,30] The MMLCT transition depletes an electron from the antibonding dσ* orbital and adds the electron density to the antibonding π* ligand-centered

Received: April 20, 2021
Accepted: July 12, 2021

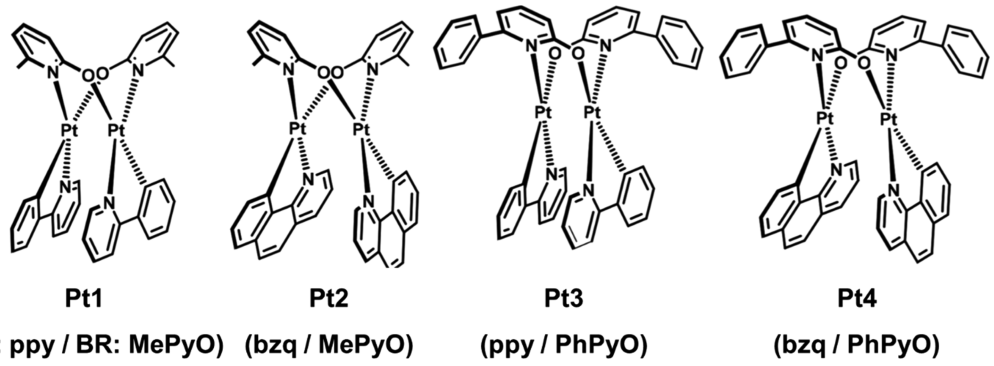

Figure 1. Molecular structures of the Pt(II) dimers investigated in this study. These 2-hydroxypyridyl-bridged Pt(II) dimeric complexes feature substantial variations in the cyclometalating (CM) and bridging (BR) ligands: 2-phenylpyridine (ppy, **Pt1** and **Pt3**) vs 7,8-benzoquinoline (bzq, **Pt2** and **Pt4**) and 2-hydroxy-6-methylpyridine (MePyO, **Pt1** and **Pt2**) vs 2-hydroxy-6-phenylpyridine (PhPyO, **Pt3** and **Pt4**).

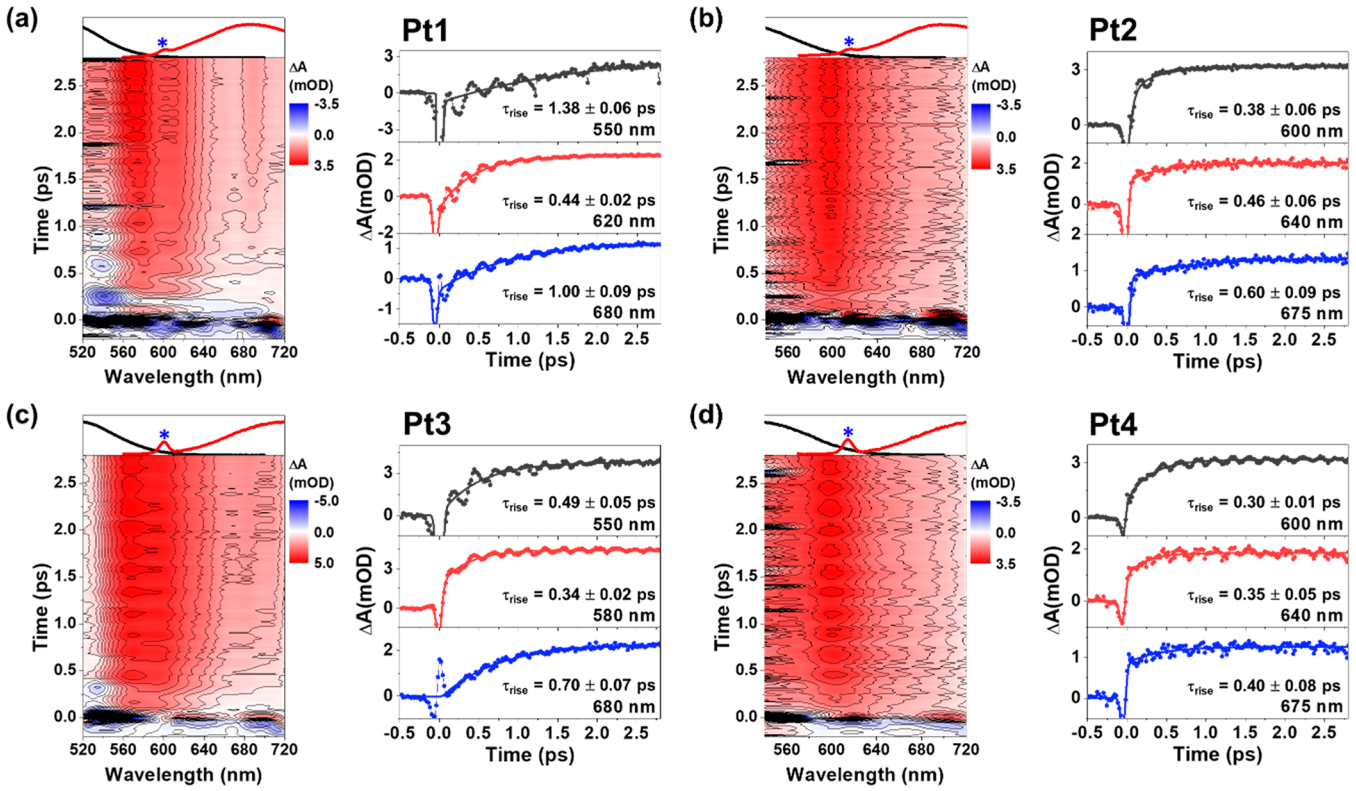

Figure 2. Femtosecond TA data maps along with absorption (^{1}MMLCT, black solid) and phosphorescence spectra (^{3}MMLCT, red solid) and their kinetic traces at specific probe wavelengths for Pt(II) dimers: (a) **Pt1**, (b) **Pt2**, (c) **Pt3**, and (d) **Pt4**. All TA measurements were performed in THF at room temperature. Asterisks indicate the Raman peaks of THF.

orbital, thereby effectively increasing the Pt−Pt bond order by ∼0.5 and shortening the Pt−Pt distance by ∼0.3−0.5 Å in the MMLCT excited state.[31,32] Consequently, the Pt−Pt stretching vibrational frequency will be higher in the excited state than in the ground state. Studies of other Pt(II) dimer complexes, such as $Pt_2(pop)_4$, also detected CVWP motions of the Pt−Pt stretching as well as its vibrational frequency increase in the excited state due to a similar mechanism, although the nature of the excited state is different.[33−35] These observations lead to a hypothesis that the Pt−Pt distance could be one of the key structural factors to be used to follow the ISC dynamics. Thus, CVWP motions of the Pt−Pt stretching mode can be a probe to reveal the excited-state trajectories of these dimers, especially for the femtosecond ISC processes.

Here, using femtosecond transient absorption (TA) spectroscopy (35 fs pulse duration), we investigated the Pt−Pt stretching CVWP dynamics during the ISC processes in a set of structurally correlated Pt(II) dimers (Figure 1).[36] The TA spectra of the four Pt(II) dimer complexes, upon photoexcitation at the ^{1}MMLCT band (λ_{ex} = 540 nm), are shown in Figure 2. Details about the electronic transitions of **Pt1**−**Pt4** are provided in Figure S1. The CVWP motions of the Pt−Pt stretching mode launched by the 35 fs photoexcitation pulses appear as oscillatory signals superimposed on the time evolution of the excited-state population (Figure 2). A broad and structureless excited-state absorption (ESA) feature in the range of ∼560−640 nm extending over the entire probe spectral range (520−720 nm) is consistent with the nanosecond ESA spectral feature from the ^{3}MMLCT state for these

https://doi.org/10.1021/acs.jpclett.1c01289
J. Phys. Chem. Lett. XXXX, XXX, XXX−XXX

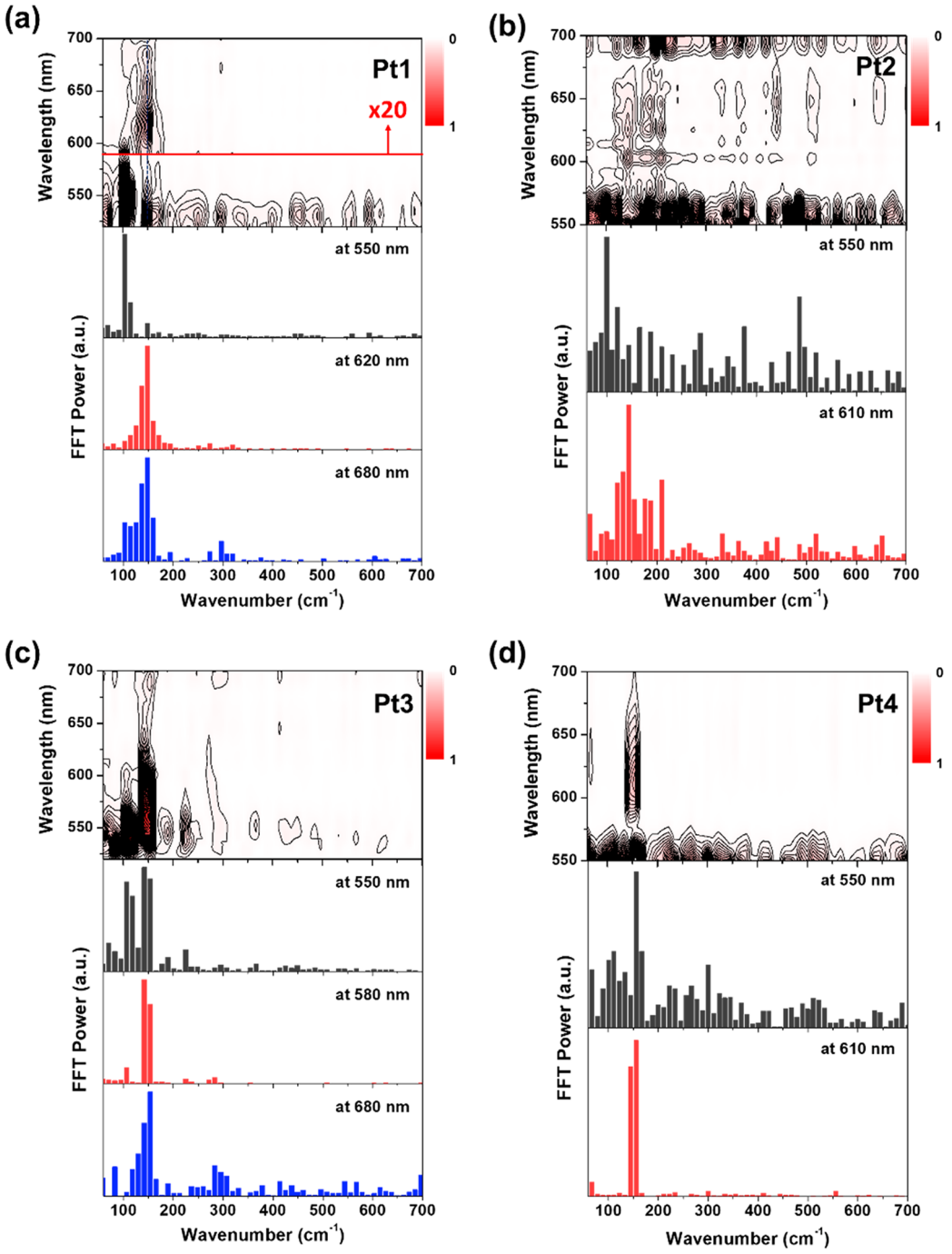

Figure 3. FFT power maps and spectra for (a) **Pt1**, (b) **Pt2**, (c) **Pt3**, and (d) **Pt4** at selected probe wavelengths as labeled. The FTs with respect to the pump−probe delay time of ≳150 fs have been processed to avoid the coherent spike and the cross-phase modulation signals around time zero.

molecules.[36] The ESA signals for all complexes rise within ∼3 ps of the excitation and then remain nearly static over the 30 ps experimental time window (Figure S6), attributed to the initial ultrafast ISC and the latter long-lived (i.e., several hundred nanoseconds) ^{3}MMLCT-state absorption features, respectively.[36]

The TA kinetic traces with delays of ≲3 ps for all Pt(II) dimers were fitted by a sum of exponential functions convoluted with a Gaussian IRF (full width at half-maximum of ∼35 fs). As shown in Figure 2, the rise kinetic time constants at three probe wavelengths were obtained using a long decay time constant fixed at 100 ns. A rise-time component shorter than the IRF was excluded due to a coherent spike and a cross-phase modulation near the delay time zero. All Pt(II) dimers exhibited a rise kinetics with a time constant of 0.3−0.4 ps around 600 nm. Additionally, **Pt1** and **Pt3** showed rise kinetics with a longer time constant (∼0.7−1.0 ps) around the redder ESA region (e.g., 680 nm), which was also identified in the decay-associated spectra (DAS, shown in Figure S7). Although the ESA signal appeared in the entire probe spectral range for all Pt(II) dimers, the TA rise traces could be attributed to a decay of stimulated emission (SE) from the ^{1}MMLCT state that is expected to appear in the range of 560−680 nm as detected in a closely related

https://doi.org/10.1021/acs.jpclett.1c01289
J. Phys. Chem. Lett. XXXX, XXX, XXX−XXX

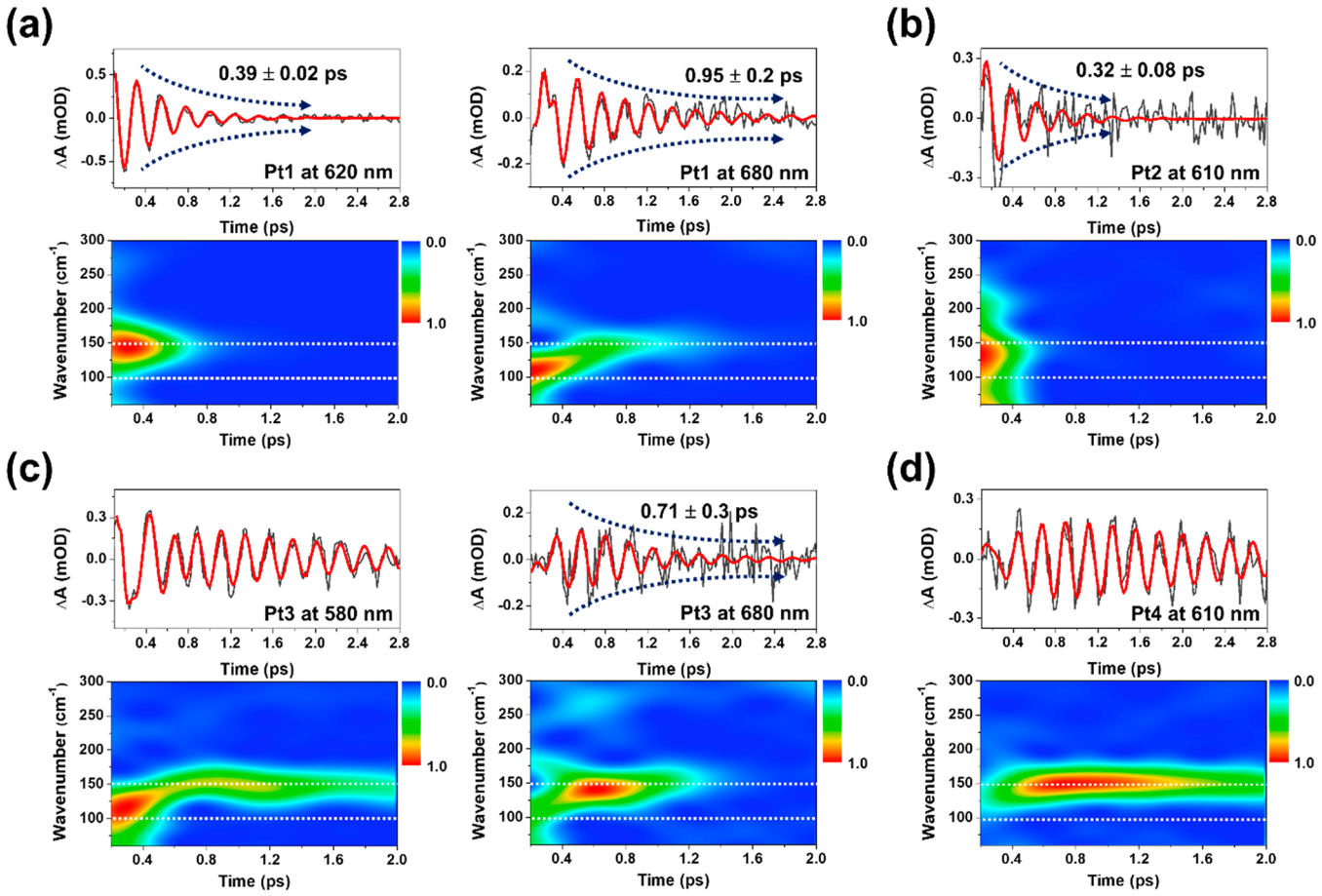

Figure 4. Oscillatory components (black) with the fit (red) to an exponentially damped sine function at the selected probe wavelengths and STFT obtained by sliding a 600 fs time window (two-dimensional contour) along the probe delay time for (a) **Pt1**, (b) **Pt2**, (c) **Pt3**, and (d) **Pt4**. Details for the fit of the oscillatory signals can be found in the Supporting Information.

pyrazolate-bridged Pt(II) dimer {[Pt(ppy)(μ-^{t}Bu$_2$pz)]$_2$} complex by femtosecond fluorescence upconversion measurements.[37] There was no sufficiently evident SE signal from our femtosecond TA spectra that could be used to unambiguously identify the SE signals from the ^{1}MMLCT state, and hence, we would focus on analyzing the CVWP motions and correlating their dynamics with the TA rise kinetics to reveal the ISC trajectories from the singlet to the triplet MMLCT state.

To identify the frequencies of the CVWP motions detected in the TA measurements, we performed fast Fourier transformation (FFT) analysis of the oscillatory signals extracted as the residuals from the excited-state population dynamics. The FFT power maps and spectra (Figure 3) reveal two dominant frequencies, ∼100 and ∼150 cm^{-1}. In all four dimers, the ∼100 cm^{-1} mode was mostly detected in the ground-state absorption region (520−560 nm),[37,38] while the ∼150 cm^{-1} mode is distributed differently across the probe spectral region. Thus, the results match the scenario described above, in which the MMLCT transition effectively shortens the Pt−Pt distance[28,31,32] and effectively increases the force constants for the Pt−Pt stretching in the excited state to produce the ∼150 cm^{-1} mode that reflects motions in the excited MMLCT-state PESs. Meanwhile, the impulsive stimulated Raman scattering (ISRS) induces the ∼100 cm^{-1} Pt−Pt stretching CVWP motions in the ground-state PESs corresponding to a longer Pt−Pt distance. Such a Pt−Pt distance difference between the ground and excited MMLCT states has been captured by previous X-ray transient absorption and scattering studies of the closely related pyrazolate-bridged Pt(II) dimers.[31,32] An upshift of the excited-state Pt−Pt stretching frequency was also observed in femtosecond TA experiments on the prototypical Pt$_2$(pop)$_4$, although its electronic transition (dσ^* → pσ) is distinctively different from that of the Pt(II) dimers investigated here.[33,35] Normal mode analysis performed for the ground- and excited-state (i.e., ^{1}MMLCT and ^{3}MMLCT) structures of these Pt(II) dimers further supported the idea that the two dominating frequencies of ∼100 and ∼150 cm^{-1} originate from the ground- and excited-state MMLCT PESs, respectively (shown in Figures S2−S5 with atomic motion vectors for those modes in the range of 100−150 cm^{-1}). The calculated Pt−Pt stretching vibrations for all Pt(II) dimers exhibited an increase in frequency from 114−120 cm^{-1} in the ground state to 138−150 cm^{-1} in both singlet and triplet MMLCT states, which confirms the assignment of the ∼150 cm^{-1} frequency to the CVWP motion in the excited PES of the MMLCT state.

As the correlation between the Pt−Pt vibrational stretching frequency and the Pt−Pt distance is established, we are able to glean insight into the ISC trajectories in the Pt(II) dimer series by following the temporal and spectral evolution of the ∼150 cm^{-1} mode from the initially populated Franck−Condon state to the ^{3}MMLCT state. A short-time Fourier transformation (STFT) analysis with a time interval of 600 fs was performed

https://doi.org/10.1021/acs.jpclett.1c01289
J. Phys. Chem. Lett. XXXX, XXX, XXX−XXX

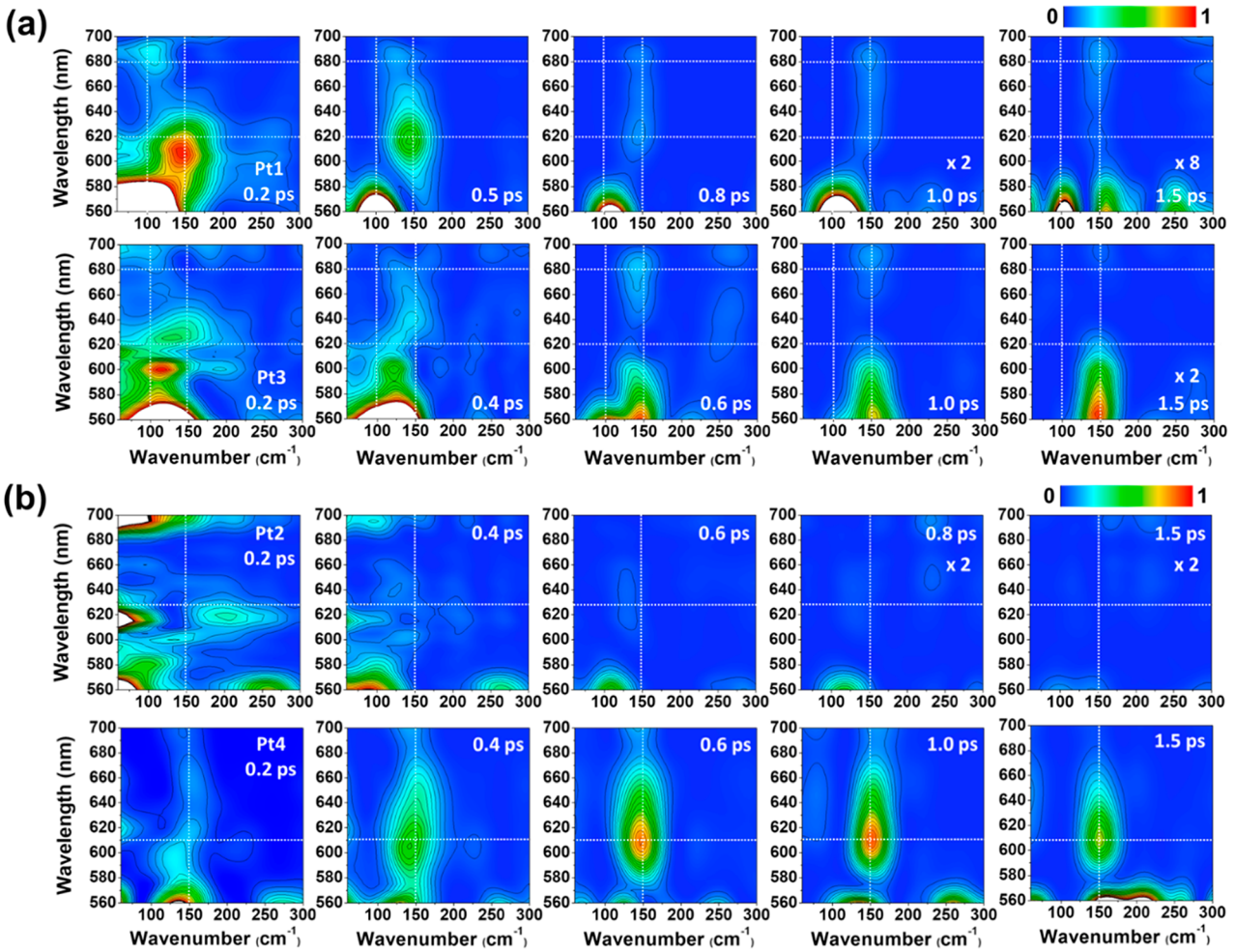

Figure 5. STFT maps for (a) **Pt1** (top) and **Pt3** (bottom) and (b) **Pt2** (top) and **Pt4** (bottom).

to take snapshots of the beating frequencies and amplitudes in the entire experimental probe spectral and delay time range. Therefore, the temporal evolution of the frequency spectra can be extracted and displayed as a function of the delay time within the boundary of the time−frequency uncertainty relation (Figure 4). Details of the STFT procedure are given in Figure S8.

The STFT analyses in Figure 4 reveal primarily two characteristics of the observed ∼150 cm^{-1} oscillatory signal. First, the long-lived CVWP beyond the ∼3 ps time delay is observed in only **Pt3** and **Pt4**. Although the CVWP dephasing time of ∼0.7 ps at 680 nm in **Pt3** is similar to the rise time constant in the TA kinetics, that at 580 nm is drastically prolonged over an ∼3 ps time window, much longer than the rise TA kinetics (Figure 2c). Similarly, a long CVWP dephasing time is also observed at 610 nm in **Pt4**. Because the phenyl groups are attached to the bridging ligands in only **Pt3** and **Pt4**, they could play an important role in the ISC trajectory, which will be discussed below. In comparison, the amplitude of the 150 cm^{-1} CVWP motions in **Pt1** decays with time constants of 0.4 ps at 620 nm and 1.0 ps at 680 nm, and that in **Pt2** at 610 nm decays even faster with a dephasing time of 0.3 ps. These time constants match the TA rise time constants for **Pt1** and **Pt2** at similar probe wavelengths (Figure 2a,c). Second, the oscillatory frequency changes concurrently with the oscillation amplitude rise at very early probe delay times. The amplitude of the 150 cm^{-1} oscillations at 680 nm in **Pt1** (Figure 4a) rises as the frequency increases from ∼100 to 150 cm^{-1} within 0.6 ps, which is comparable to the CVWP dephasing time detected at 620 nm. Similarly, the amplitude of the 150 cm^{-1} oscillation at 680 nm in **Pt3** increases within 0.6 ps. While **Pt3** has a prolonged CVWP dephasing time (>3 ps) at 580 nm, the 150 cm^{-1} oscillatory amplitude increases as the oscillation frequency increases (from ∼100 to ∼150 cm^{-1}), also detected in the early delay time (Figure 4c). Similar to **Pt3** (Figure 4b), the prolonged 150 cm^{-1} CVWP motion at 610 nm in **Pt4** (Figure 4d) exhibits amplitude growth with a frequency upshift from ∼100 to 150 cm^{-1}. The frequency changes observed in **Pt3** (at 580 nm) and **Pt4** (at 610 nm) are most likely attributed to the ∼100 cm^{-1} CVWP motion generated in the ground state by the ISRS.

While the amplitude time evolution for the CVWP motions of the Pt−Pt stretching at 150 cm^{-1} reflects the excited-state population dynamics on the excited-state PESs, the spectral evolution of this mode captures the energetic trajectory of the excited state. The STFT spectra as a function of probe wavelength, as shown in Figure 5, correlate the time evolution of the Pt−Pt stretching CVWP motions with the TA spectral changes related to the ISC, thereby tracking the ISC trajectories.

In the probe range of 620−700 nm, the STFT maps for **Pt1** and **Pt3** clearly reveal a red-shift of the 150 cm^{-1} amplitude distribution from ∼620 to ∼680 nm (Figure 5a). Such an obvious spectral change was not detected in the entire TA

https://doi.org/10.1021/acs.jpclett.1c01289
J. Phys. Chem. Lett. XXXX, XXX, XXX−XXX

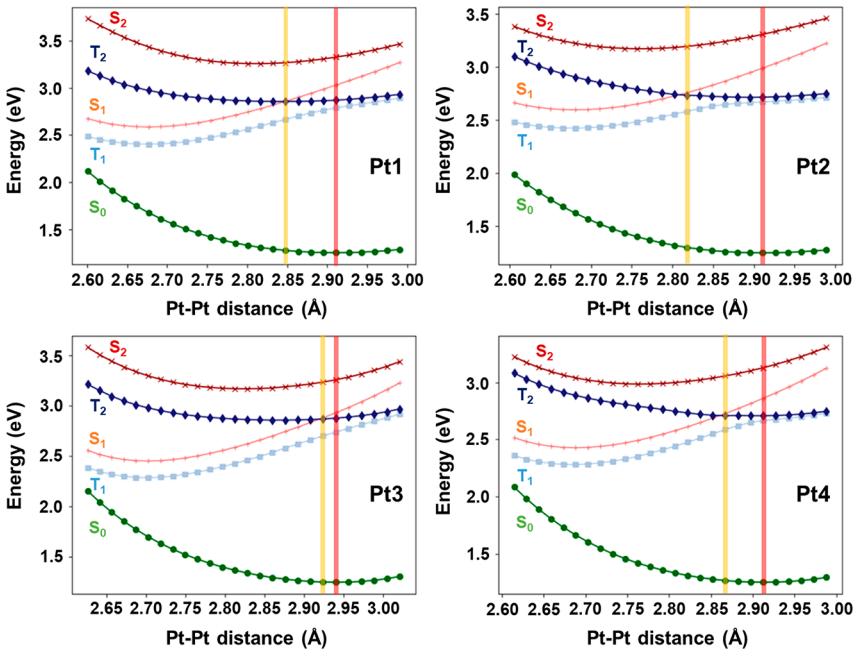

Figure 6. Calculated PESs for all Pt(II) dimers projected as a function of Pt−Pt distance. Abbreviations: S_0, ground state; S_1, ^{1}MMLCT state; T_2, ligand-centered triplet state; T_1, ^{3}MMLCT state. Red bars indicate the Franck−Condon regime, while yellow bars show the conical intersection between S_1 and T_2.

probe range where the ESA of the ^{3}MMLCT state prevails (Figure 2). After the red-shift, the 150 cm^{-1} CVWP motion dephases with time constants of ∼1.0 ps for **Pt1** and ∼0.7 ps for **Pt3**, quantitatively matching the TA rise kinetics associated with the ISC (Figure 1a,c). These spectral and temporal behaviors in **Pt1** and **Pt3** strongly indicate that the 150 cm^{-1} CVWP dynamics detected in range of 620−700 nm originate from the population dynamics on the ^{1}MMLCT PES. It has been shown in the pyrazolate-bridged Pt(II) dimer that the ISC process induces the dephasing of the Pt−Pt stretching CVWP in the ^{1}MMLCT state.[37] Thus, the red-shift of the 150 cm^{-1} amplitude distribution likely comes from the vibrational relaxation from the higher to lower vibrational levels in the PES of the ^{1}MMLCT state during the ISC. Correlating the spectral and temporal evolution of the 150 cm^{-1} CVWP with the observed TA rise kinetics, the shorter and longer TA rise traces detected around 600 and 680 nm in **Pt1** and **Pt3** [0.3−0.4 and 0.7−1.0 ps, respectively (Figure 2a,c)], can be attributed to the vibrational relaxation and the ISC (^{1}MMLCT → ^{3}MMLCT) dynamics, respectively. There is no direct evidence to identify whether the 150 cm^{-1} CVWP in range of 620−700 nm originates from the ESA or SE of the ^{1}MMLCT state, but the results are aligned with those of a study of a similar Pt(II) dimer with the fluorescence decay from the ^{1}MMLCT state in range of 550−650 nm using the fluorescence upconversion method.[37] Furthermore, because the vibrational relaxation dynamics induce a blue-shift of the ESA, the red-shift in the spectra and the corresponding temporal changes of the 150 cm^{-1} CVWP in range of 620−700 nm for **Pt1** and **Pt3** likely originate from the SE dynamics of the ^{1}MMLCT state.

In the STFT maps of **Pt3** (Figure 5a, bottom panels), the ∼150 cm^{-1} CVWP motion detected in the range of 560−600 nm exhibits a time evolution very different from that in the probe region of 620−700 nm. The 150 cm^{-1} oscillatory amplitude for **Pt3** in the range of 560−600 nm has not only a long dephasing time (>3 ps) but also rise kinetics occurring within 0.6 ps of the pump pulse (Figure S10b). The lasting vibrational coherence beyond the TA rise times (0.3 and 0.7 ps) strongly suggests that the 150 cm^{-1} CVWP motion in the range of 560−600 nm occurs on the PES of the ^{3}MMLCT state, because the CVWP motion in the ^{1}MMLCT PES (observed in the probe range of 620−700 nm) decays with a time constant of 0.7 ps. In addition, the normal mode analyses support the idea that the Pt−Pt stretching CVWP in the ^{3}MMLCT state has a frequency similar to that of the ^{1}MMLCT state (Figures S2−S5). Furthermore, because the ^{3}MMLCT state is detected only by the ESA signals, the oscillation amplitude rise measured within 0.6 ps reflects the growth of the ^{3}MMLCT population through ISC. Overall, the long-lasting 150 cm^{-1} oscillation in the range of 560−600 nm strongly indicates that the Pt−Pt stretching CVWP that initially populated the ^{1}MMLCT PES of **Pt3** is partially retained during the ISC to the ^{3}MMLCT state.

The early STFT maps of **Pt2** (Figure 5b) reveal a weak amplitude for the ∼150 cm^{-1} mode at 630 nm, dephasing in ∼0.4 ps, concurrent with the rise time in the TA traces (Figure 4b). Although it is unclear whether this oscillation amplitude at 630 nm originates from the SE or the ESA signal of the ^{1}MMLCT state, the consistency between the dephasing and TA rise time provides strong evidence to correlate the CVWP dynamics with the ISC. As a comparison, the 150 cm^{-1} CVWP motions in the STFT maps for **Pt4** feature a large amplitude around 590−660 nm with a >3 ps time window and an ∼0.6 ps rise time (Figure 5b and Figure S10c), which is similar to the TA rise kinetics (Figure 4d and Figure S8). Hence, the amplitude growth and the long dephasing time beyond the TA rise time suggest the retention of the Pt−Pt stretching CVWP motions in **Pt4** during the ISC.

The STFT analyses showed the Pt−Pt stretching CVWP in **Pt3** and **Pt4** is retained during the ISC process. To determine detailed ISC trajectories, the PESs of ground state S_0 and

https://doi.org/10.1021/acs.jpclett.1c01289
J. Phys. Chem. Lett. XXXX, XXX, XXX−XXX

lower-energy excited states for the four Pt(II) dimers were calculated and projected as a function of the Pt−Pt distance (Figure 6). The shapes and energies of these PESs provide insight into the ISC trajectories and rationalization of the experimentally detected behaviors of the Pt−Pt stretching CVWP. Notably, in the Franck−Condon (FC) region (Figure 6, vertical red bar), there is an intermediate state, T_2 (^{3}LC, CM ligand-localized triplet state), with its energy between those of the S_1 (^{1}MMLCT) and T_1 (^{3}MMLCT) states. Thus, T_2 is a plausible intermediate state that may play a role in the retention of the Pt−Pt stretching CVWP in the ISC process. Such a T_2 state has been also identified in a previous theoretical study.[39] The calculated PESs in Figure 6 clearly show the effects of ligand substitution. (a) The energy of the S_1 PES is decreased in **Pt3** and **Pt4** with the phenyl groups in the bridging ligands, and (b) the T_2 PES is steeper in **Pt2** and **Pt4** with larger aromatic CM ligands. The effect from step a brings the conical intersection (CI, vertical yellow bar) between S_1 and T_2 near the FC region, and that from step b makes the T_2 and T_1 PESs nearly isoenergetic in the FC region. Consequently, S_1 could proceed via two different routes leading to T_1: (1) S_1 ($\nu = n$; $n > 0$) → S_1 ($\nu = 0$) → T_1 or (2) S_1 ($\nu = n$; $n > 0$) → T_2 → T_1. In particular, the CI of S_1 and T_2 in the PES suggests that the initial Pt−Pt stretching CVWP could be retained from S_1 to T_2 near the FC region. Hence, the Pt−Pt stretching CVWP retention revealed by the STFT analyses for **Pt3** and **Pt4** would be operative via the second ISC pathway [S_1 ($\nu = n$; $n > 0$) → T_2 → T_1], aligned with a recent study on $Pt_2(pop)_4$ in which the Pt−Pt stretching CVWP in the S_1 state was retained in the final T_1 state via an intermediate charge transfer state.[34,35] Apparently, **Pt4** possesses an optimal situation for undergoing the second ISC pathway because both its CI of S_1 and T_2 and isoenergetic PESs of T_2 and T_1 are all near the FC region to enable the transition times from S_1 to T_1 via T_2 much shorter than the Pt−Pt stretching period of ∼220 fs, and thus to retain most of its CVWP in the final T_1 state. In comparison, **Pt3** has an optimal CI of S_1 and T_2 near the FC region, but the PES energy difference between T_2 and T_1 is slightly larger than that of **Pt4** so that it has dual pathways. Furthermore, our recent theoretical study has examined the ISC dynamics on a pyrazolate-bridged Pt(II) dimer by a fully variational relativistic method, demonstrating the consistent result that the high-lying ^{3}LC state with its energy adjacent to the ^{1}MMLCT state enables ultrafast ISC to the ^{3}MMLCT state.[40]

On the basis of the STFT analyses (Figure 5) and the calculated excited-state PESs (Figure 6), Figure 7 depicts the ISC trajectories projected onto the Pt−Pt stretching vibrational coordinate for **Pt3** and **Pt4**. The Pt−Pt stretching CVWP is first launched by the ground state to the ^{1}MMLCT PES transition at the FC region with an increased Pt−Pt bond order and a corresponding oscillation frequency of ∼150 cm^{-1} (220 fs period). In **Pt3**, the CVWP dynamics observed in the probe range of 620−700 nm corresponds to the first ISC pathway. The initial Pt−Pt stretching CVWP relaxes to lower vibrational states in the ^{1}MMLCT PES [S_1 ($\nu = n$; $n > 0$) → S_1 ($\nu = 0$) (Figure 7, blue dotted arrow)]. The CVWP subsequently dephases during ISC to the ^{3}MMLCT state because the first ISC channel is symmetry-forbidden, resulting in the population rise time constant of 0.7 ps being much longer than the oscillation period to preserve the CVWP motions. Meanwhile, some portion of the initial CVWP for **Pt3** in the FC regime follows the second ISC pathway [S_1 ($\nu = n$; $n > 0$) → T_2 → T_1 (red dotted line)], enabling the transfer of CVWP to the intermediate PES through the CI as discussed above (Figure 6). Then, the Pt−Pt stretching CVWP continues to propagate through ultrafast internal conversion to the ^{3}MMLCT state and is sustained over 3 ps as detected around the ESA band of 560−600 nm. In STFT maps, the 150 cm^{-1} oscillatory amplitude exhibited rise kinetics in the probe range of 560−600 nm (Figure 5 and Figure S10b), which is high and possibly related to the internal conversion. Although the Pt−Pt stretching CVWP dynamics related to the first ISC path is clearly undetectable in **Pt4**, the long dephasing time for the Pt−Pt stretching CVWP detected around 590−660 nm strongly supports the second ISC pathway for **Pt4**.

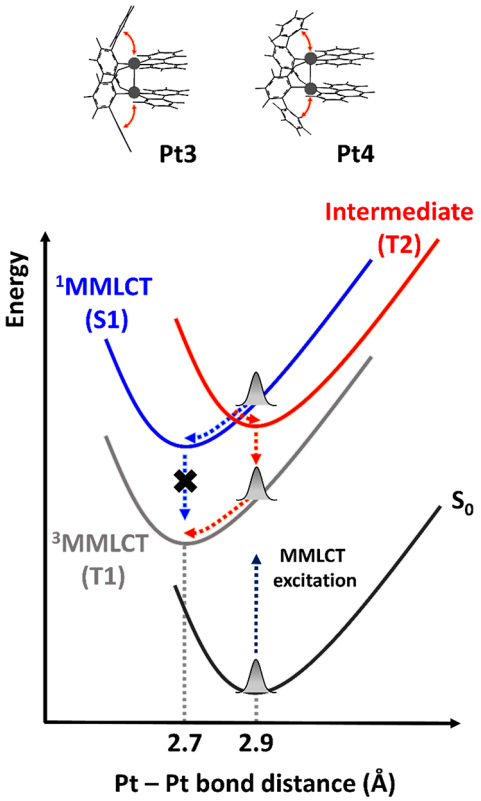

Figure 7. Proposed mechanism for Pt−Pt stretching CVWP dynamics during ISC processes in **Pt3** and **Pt4**. Blue arrows indicate the first ISC pathway [S_1 ($\nu = n$; $n > 0$) → S_1 ($\nu = 0$) → T_1], while red arrows show the second ISC path via the intermediate state [S_1 ($\nu = n$; $n > 0$) → T_2 → T_1], enabling the conservation of Pt−Pt stretching CVWP detected in both **Pt3** and **Pt4**.

The calculated PESs for **Pt1** and **Pt2** (Figure 6) also predict the CI of S_1 and T_2. However, no evidence for the conservation of the Pt−Pt stretching CVWP was shown by the STFT analyses. Apparently, the phenyl substituents on the BR ligands in **Pt3** and **Pt4** may exert influence in steering the molecule toward the second ISC trajectory. As shown in Figure 5, the pendant phenyl rings in the BR ligands of **Pt3** and **Pt4** result in decreasing the S_1 PES energy relative to that of T_2, shifting the CI closer to the FC region. As a result, the Pt−Pt distances of **Pt3** and **Pt4** at the CI are more similar to those at the FC state compared to **Pt1** and **Pt2**. Given that the retention of the Pt−Pt stretching CVWP was detected in only **Pt3** and **Pt4**, the similarity between the Pt−Pt distance in the CI and FC regions enhances the second ISC pathway. In this regard, it is noteworthy that the contraction of the Pt−Pt bond is

https://doi.org/10.1021/acs.jpclett.1c01289
J. Phys. Chem. Lett. XXXX, XXX, XXX−XXX

accompanied by two major changes of inter-CM ligand geometry from the ground-state structures (Figures S2−S5): (1) the decrease in the inter-CM ligand distance (∼0.25 Å) and (2) the decrease in the twisting angle between two planes of CM ligands (∼3.5°). The calculated excited-state structures indicate that the structural reorganization associated with inter-CM ligand geometry also becomes larger as the CI moves away from the FC region. The early STFT maps showed a short-lived ∼100 cm^{-1} CVWP near 685 nm for **Pt1** and 600 nm for **Pt3**, which is different from the ground-state CVWP with a longer dephasing time (Figure 5). Indeed, the inter-CM ligand twisting motion was identified around ∼60 cm^{-1} in the normal mode analyses, which is possibly related to the observed ∼100 cm^{-1} value (Figure S11 and details in the Supporting Information). Collectively, the observed CVWP conservation in only **Pt3** and **Pt4** suggests that the branching ratio of two ISC pathways strongly depends on the Pt−Pt distance and the related CM−ligand structure at the CI.

Therefore, the Pt−Pt stretching CVWP can be preserved by decreasing the S_1 PES energy for **Pt3** and **Pt4** as shown in Figure 6. The trend seen in the HOMO−LUMO energy gap across all Pt(II) dimers (Figure S1b) also demonstrates the effects of the ligands on the S_1 PES (Figure S1b). In addition, the HOMOs for **Pt3** and **Pt4** exhibit dσ* partially delocalized into the π* orbitals of the phenyl rings, resulting in destabilization of the HOMO energy levels and a decrease in the HOMO−LUMO energy gap associated with the MMLCT transition. The interactions between the phenyl groups in the BR ligand and Pt(II) atoms likely remain in the S_1 and T_1 states, because the Pt−Pt and Pt−phenyl ring distances become even shorter compared to those in the ground-state structure (Figures S4 and S5). A detailed computational study is currently underway to reveal the precise interplay of the Pt−Pt stretching vibration and other relevant structural components in Pt(II) dimers and their impact on spin-vibronic coupling in the second ISC process.

In summary, ultrafast ISC trajectories of structurally related Pt(II) dimer complexes (**Pt1**−**Pt4**) have been examined by transient absorption spectroscopy with a 35 fs pulse via analysis of the time evolution of the Pt−Pt stretching CVWP motions in both temporal and spectral dimensions. The results reveal the dual ISC pathways, from S_1 to T_1 directly and via an intermediate T_2 state, evidenced by the different coherent vibrational wavepacket behaviors of the Pt−Pt stretching across the four structurally related Pt(II) dimer complexes. In particular, the calculated PESs of different states indicate the importance of ligands in altering relative energies and conical intersections of different states, which enabled different reaction paths. This study presents possibilities of controlling the branching ratio between two ISC paths by the relative positions of conical intersections to the FC states using modifications of cyclometalating and bridging ligands in the Pt(II) dimer complexes. Therefore, what we have learned from structurally dependent CVWP behaviors in these Pt(II) dimer complexes can enhance our understanding of other TMC excited-state reaction trajectories to influence the outcome of various photochemical processes.

■ ASSOCIATED CONTENT

Supporting Information

The Supporting Information is available free of charge at https://pubs.acs.org/doi/10.1021/acs.jpclett.1c01289.

Ground-state absorption spectra, quantum calculation results, long-time TA kinetics, DAS, analysis for the beating signals, and instrumentation for the TA measurements (PDF)

■ AUTHOR INFORMATION

Corresponding Authors

Lin X. Chen − *Department of Chemistry, Northwestern University, Evanston, Illinois 60208, United States; Chemical Science and Engineering Division, Argonne National Laboratory, Lemont, Illinois 60439, United States;* orcid.org/0000-0002-8450-6687; Email: lchen@anl.gov, l-chen@northwestern.edu

Xiaosong Li − *Department of Chemistry, University of Washington, Seattle, Washington 98195, United States;* orcid.org/0000-0001-7341-6240; Email: xsli@uw.edu

Felix N. Castellano − *Department of Chemistry, North Carolina State University, Raleigh, North Carolina 27695-8204, United States;* orcid.org/0000-0001-7546-8618; Email: fncastel@ncsu.edu

Authors

Pyosang Kim − *Department of Chemistry, Northwestern University, Evanston, Illinois 60208, United States; Chemical Science and Engineering Division, Argonne National Laboratory, Lemont, Illinois 60439, United States*

Andrew J. S. Valentine − *Department of Chemistry, University of Washington, Seattle, Washington 98195, United States*

Subhangi Roy − *Department of Chemistry, North Carolina State University, Raleigh, North Carolina 27695-8204, United States*

Alexis W. Mills − *Department of Chemistry, University of Washington, Seattle, Washington 98195, United States*

Arnab Chakraborty − *Department of Chemistry, North Carolina State University, Raleigh, North Carolina 27695-8204, United States*

Complete contact information is available at: https://pubs.acs.org/10.1021/acs.jpclett.1c01289

Notes

The authors declare no competing financial interest.

■ ACKNOWLEDGMENTS

This work has been supported by the National Science Foundation (Grant CHE-1955806 to L.X.C. and Grant CHE-1955795 to F.N.C.). The computational work and P.K. and L.X.C. is supported in part by the Ultrafast Initiative of the U.S. Department of Energy, Office of Science, Office of Basic Energy Sciences, through Argonne National Laboratory under Contract DE-AC02-06CH11357. The development of the computational method for simulating excited-state dynamics is supported by the National Science Foundation (Grant CHE-1856210 to X.L.).

■ REFERENCES

(1) McCusker, J. K. Electronic structure in the transition metal block and its implications for light harvesting. *Science* **2019**, *363*, 484.

(2) Mara, M. W.; Bowman, D. N.; Buyukcakir, O.; Shelby, M. L.; Haldrup, K.; Huang, J.; Harpham, M. R.; Stickrath, A. B.; Zhang, X.; Stoddart, J. F.; Coskun, A.; Jakubikova, E.; Chen, L. X. Electron Injection from Copper Diimine Sensitizers into TiO2: Structural Effects and Their Implications for Solar Energy Conversion Devices. *J. Am. Chem. Soc.* **2015**, *137*, 9670−9684.

(3) Harlang, T. C. B.; Liu, Y.; Gordivska, O.; Fredin, L. A.; Ponseca, C. S.; Huang, P.; Chábera, P.; Kjaer, K. S.; Mateos, H.; Uhlig, J.; Lomoth, R.; Wallenberg, R.; Styring, S.; Persson, P.; Sundström, V.; Wärnmark, K. Iron sensitizer converts light to electrons with 92% yield. *Nat. Chem.* **2015**, *7*, 883−889.
(4) Twilton, J.; Le, C.; Zhang, P.; Shaw, M. H.; Evans, R. W.; MacMillan, D. W. C. The merger of transition metal and photocatalysis. *Nat. Rev. Chem.* **2017**, *1*, 0052.
(5) Arias-Rotondo, D. M.; McCusker, J. K. The photophysics of photoredox catalysis: a roadmap for catalyst design. *Chem. Soc. Rev.* **2016**, *45*, 5803−5820.
(6) Wenger, O. S. Photoactive Complexes with Earth-Abundant Metals. *J. Am. Chem. Soc.* **2018**, *140*, 13522−13533.
(7) Kalyanasundaram, K.; Grätzel, M. Applications of functionalized transition metal complexes in photonic and optoelectronic devices. *Coord. Chem. Rev.* **1998**, *177*, 347−414.
(8) Dalle, K. E.; Warnan, J.; Leung, J. J.; Reuillard, B.; Karmel, I. S.; Reisner, E. Electro- and Solar-Driven Fuel Synthesis with First Row Transition Metal Complexes. *Chem. Rev.* **2019**, *119*, 2752−2875.
(9) Huse, N.; Kim, T. K.; Jamula, L.; McCusker, J. K.; de Groot, F. M. F.; Schoenlein, R. W. Photo-Induced Spin-State Conversion in Solvated Transition Metal Complexes Probed via Time-Resolved Soft X-ray Spectroscopy. *J. Am. Chem. Soc.* **2010**, *132*, 6809−6816.
(10) Zhang, W.; Alonso-Mori, R.; Bergmann, U.; Bressler, C.; Chollet, M.; Galler, A.; Gawelda, W.; Hadt, R. G.; Hartsock, R. W.; Kroll, T.; Kjær, K. S.; Kubiček, K.; Lemke, H. T.; Liang, H. W.; Meyer, D. A.; Nielsen, M. M.; Purser, C.; Robinson, J. S.; Solomon, E. I.; Sun, Z.; Sokaras, D.; van Driel, T. B.; Vankó, G.; Weng, T.-C.; Zhu, D.; Gaffney, K. J. Tracking excited-state charge and spin dynamics in iron coordination complexes. *Nature* **2014**, *509*, 345−348.
(11) Lemke, H. T.; Kjær, K. S.; Hartsock, R.; van Driel, T. B.; Chollet, M.; Glownia, J. M.; Song, S.; Zhu, D.; Pace, E.; Matar, S. F.; Nielsen, M. M.; Benfatto, M.; Gaffney, K. J.; Collet, E.; Cammarata, M. Coherent structural trapping through wave packet dispersion during photoinduced spin state switching. *Nat. Commun.* **2017**, *8*, 15342.
(12) Katayama, T.; Northey, T.; Gawelda, W.; Milne, C. J.; Vankó, G.; Lima, F. A.; Bohinc, R.; Németh, Z.; Nozawa, S.; Sato, T.; Khakhulin, D.; Szlachetko, J.; Togashi, T.; Owada, S.; Adachi, S.-i.; Bressler, C.; Yabashi, M.; Penfold, T. J. Tracking multiple components of a nuclear wavepacket in photoexcited Cu(I)-phenanthroline complex using ultrafast X-ray spectroscopy. *Nat. Commun.* **2019**, *10*, 3606.
(13) Cho, S.; Mara, M. W.; Wang, X.; Lockard, J. V.; Rachford, A. A.; Castellano, F. N.; Chen, L. X. Coherence in Metal−Metal-to-Ligand-Charge-Transfer Excited States of a Dimetallic Complex Investigated by Ultrafast Transient Absorption Anisotropy. *J. Phys. Chem. A* **2011**, *115*, 3990−3996.
(14) Iwamura, M.; Takeuchi, S.; Tahara, T. Ultrafast Excited-State Dynamics of Copper(I) Complexes. *Acc. Chem. Res.* **2015**, *48*, 782−791.
(15) Auböck, G.; Chergui, M. Sub-50-fs photoinduced spin crossover in [Fe(bpy)3]2+. *Nat. Chem.* **2015**, *7*, 629−633.
(16) Gaynor, J. D.; Sandwisch, J.; Khalil, M. Vibronic coherence evolution in multidimensional ultrafast photochemical processes. *Nat. Commun.* **2019**, *10*, 5621.
(17) Schrauben, J. N.; Dillman, K. L.; Beck, W. F.; McCusker, J. K. Vibrational coherence in the excited state dynamics of Cr(acac)3: probing the reaction coordinate for ultrafast intersystem crossing. *Chemical Science* **2010**, *1*, 405−410.
(18) Wächtler, M.; Guthmuller, J.; Kupfer, S.; Maiuri, M.; Brida, D.; Popp, J.; Rau, S.; Cerullo, G.; Dietzek, B. Ultrafast Intramolecular Relaxation and Wave-Packet Motion in a Ruthenium-Based Supramolecular Photocatalyst. *Chem. - Eur. J.* **2015**, *21*, 7668−7674.
(19) Iwamura, M.; Nozaki, K.; Takeuchi, S.; Tahara, T. Real-Time Observation of Tight Au−Au Bond Formation and Relevant Coherent Motion upon Photoexcitation of [Au(CN)2−] Oligomers. *J. Am. Chem. Soc.* **2013**, *135*, 538−541.
(20) Scholes, G. D.; Fleming, G. R.; Chen, L. X.; Aspuru-Guzik, A.; Buchleitner, A.; Coker, D. F.; Engel, G. S.; van Grondelle, R.; Ishizaki, A.; Jonas, D. M.; Lundeen, J. S.; McCusker, J. K.; Mukamel, S.; Ogilvie, J. P.; Olaya-Castro, A.; Ratner, M. A.; Spano, F. C.; Whaley, K. B.; Zhu, X. Using coherence to enhance function in chemical and biophysical systems. *Nature* **2017**, *543*, 647−656.
(21) Paulus, B. C.; Adelman, S. L.; Jamula, L. L.; McCusker, J. K. Leveraging excited-state coherence for synthetic control of ultrafast dynamics. *Nature* **2020**, *582*, 214−218.
(22) Evans, R. C.; Douglas, P.; Winscom, C. J. Coordination complexes exhibiting room-temperature phosphorescence: Evaluation of their suitability as triplet emitters in organic light emitting diodes. *Coord. Chem. Rev.* **2006**, *250*, 2093−2126.
(23) Ho, C.-L.; Wong, W.-Y.; Yao, B.; Xie, Z.; Wang, L.; Lin, Z. Synthesis, characterization, photophysics and electrophosphorescent applications of phosphorescent platinum cyclometalated complexes with 9-arylcarbazole moieties. *J. Organomet. Chem.* **2009**, *694*, 2735−2749.
(24) Chaaban, M.; Zhou, C.; Lin, H.; Chyi, B.; Ma, B. Platinum(ii) binuclear complexes: molecular structures, photophysical properties, and applications. *J. Mater. Chem. C* **2019**, *7*, 5910−5924.
(25) Ma, B.; Li, J.; Djurovich, P. I.; Yousufuddin, M.; Bau, R.; Thompson, M. E. Synthetic Control of Pt···Pt Separation and Photophysics of Binuclear Platinum Complexes. *J. Am. Chem. Soc.* **2005**, *127*, 28−29.
(26) Rachford, A. A.; Castellano, F. N. Thermochromic Absorption and Photoluminescence in [Pt(ppy)(μ-Ph2pz)]2. *Inorg. Chem.* **2009**, *48*, 10865−10867.
(27) Chakraborty, A.; Deaton, J. C.; Haefele, A.; Castellano, F. N. Charge-Transfer and Ligand-Localized Photophysics in Luminescent Cyclometalated Pyrazolate-Bridged Dinuclear Platinum(II) Complexes. *Organometallics* **2013**, *32*, 3819−3829.
(28) Han, M.; Tian, Y.; Yuan, Z.; Zhu, L.; Ma, B. A Phosphorescent Molecular "Butterfly" that undergoes a Photoinduced Structural Change allowing Temperature Sensing and White Emission. *Angew. Chem., Int. Ed.* **2014**, *53*, 10908−10912.
(29) Zhou, C.; Yuan, L.; Yuan, Z.; Doyle, N. K.; Dilbeck, T.; Bahadur, D.; Ramakrishnan, S.; Dearden, A.; Huang, C.; Ma, B. Phosphorescent Molecular Butterflies with Controlled Potential-Energy Surfaces and Their Application as Luminescent Viscosity Sensor. *Inorg. Chem.* **2016**, *55*, 8564−8569.
(30) Brown-Xu, S. E.; Kelley, M. S. J.; Fransted, K. A.; Chakraborty, A.; Schatz, G. C.; Castellano, F. N.; Chen, L. X. Tunable Excited-State Properties and Dynamics as a Function of Pt−Pt Distance in Pyrazolate-Bridged Pt(II) Dimers. *J. Phys. Chem. A* **2016**, *120*, 543−550.
(31) Lockard, J. V.; Rachford, A. A.; Smolentsev, G.; Stickrath, A. B.; Wang, X.; Zhang, X.; Atenkoffer, K.; Jennings, G.; Soldatov, A.; Rheingold, A. L.; Castellano, F. N.; Chen, L. X. Triplet Excited State Distortions in a Pyrazolate Bridged Platinum Dimer Measured by X-ray Transient Absorption Spectroscopy. *J. Phys. Chem. A* **2010**, *114*, 12780−12787.
(32) Haldrup, K.; Dohn, A. O.; Shelby, M. L.; Mara, M. W.; Stickrath, A. B.; Harpham, M. R.; Huang, J.; Zhang, X.; Møller, K. B.; Chakraborty, A.; Castellano, F. N.; Tiede, D. M.; Chen, L. X. Butterfly Deformation Modes in a Photoexcited Pyrazolate-Bridged Pt Complex Measured by Time-Resolved X-Ray Scattering in Solution. *J. Phys. Chem. A* **2016**, *120*, 7475−7483.
(33) van der Veen, R. M.; Cannizzo, A.; van Mourik, F.; Vlček, A.; Chergui, M. Vibrational Relaxation and Intersystem Crossing of Binuclear Metal Complexes in Solution. *J. Am. Chem. Soc.* **2011**, *133*, 305−315.
(34) Monni, R.; Auböck, G.; Kinschel, D.; Aziz-Lange, K. M.; Gray, H. B.; Vlček, A.; Chergui, M. Conservation of vibrational coherence in ultrafast electronic relaxation: The case of diplatinum complexes in solution. *Chem. Phys. Lett.* **2017**, *683*, 112−120.
(35) Monni, R.; Capano, G.; Auböck, G.; Gray, H. B.; Vlček, A.; Tavernelli, I.; Chergui, M. Vibrational coherence transfer in the

https://doi.org/10.1021/acs.jpclett.1c01289
J. Phys. Chem. Lett. XXXX, XXX, XXX−XXX

ultrafast intersystem crossing of a diplatinum complex in solution. *Proc. Natl. Acad. Sci. U. S. A.* **2018**, *115*, No. E6396.
(36) Chakraborty, A.; Yarnell, J. E.; Sommer, R. D.; Roy, S.; Castellano, F. N. Excited-State Processes of Cyclometalated Platinum-(II) Charge-Transfer Dimers Bridged by Hydroxypyridines. *Inorg. Chem.* **2018**, *57*, 1298−1310.
(37) Mewes, L.; Ingle, R. A.; Megow, S.; Böhnke, H.; Baranoff, E.; Temps, F.; Chergui, M. Ultrafast Intersystem Crossing and Structural Dynamics of [Pt(ppy)(μ-tBu2pz)]2. *Inorg. Chem.* **2020**, *59*, 14643−14653.
(38) Kim, P.; Kelley, M. S.; Chakraborty, A.; Wong, N. L.; Van Duyne, R. P.; Schatz, G. C.; Castellano, F. N.; Chen, L. X. Coherent Vibrational Wavepacket Dynamics in Platinum(II) Dimers and Their Implications. *J. Phys. Chem. C* **2018**, *122*, 14195−14204.
(39) Saito, K.; Nakao, Y.; Sakaki, S. Theoretical Study of Pyrazolate-Bridged Dinuclear Platinum(II) Complexes: Interesting Potential Energy Curve of the Lowest Energy Triplet Excited State and Phosphorescence Spectra. *Inorg. Chem.* **2008**, *47*, 4329−4337.
(40) Valentine, A. J. S.; Radler, J. J.; Mills, A.; Kim, P.; Castellano, F. N.; Chen, L. X.; Li, X. Resolving the ultrafast intersystem crossing in a bimetallic platinum complex. *J. Chem. Phys.* **2019**, *151*, 114303.

https://doi.org/10.1021/acs.jpclett.1c01289
J. Phys. Chem. Lett. XXXX, XXX, XXX−XXX